Predicting Stall of a Two-dimensional Airfoil Using an Algebraic Reynolds Stress Model

L. Davidson
CERFACS
42, Av. Gustave Coriolis
31057 Toulouse
FRANCE
Report TR/RF/91/52, 1991

1 Introduction

In the Computational Aerodynamic Team at **CERFACS** work is going on calculating the flow around low-speed high-lift two-dimensional airfoils ($R_e = 2.1 \times 10^6$; $M = 0.15$) with the object to be able to predict stall. Work has been carried out improving the numerical scheme [1], as well as implementing and testing different turbulence models, such as the Baldwin-Lomax model and various $k - \varepsilon$ models [2,3]. The main problem in these works was that the separation zone near the trailing edge was much under-predicted compared with experiments, and when the angle of attack was increased the predicted lift coefficient increased even though the experiments show that stall should occur. It was believed that this failure of predicting stall could be due to inadequate turbulence models.

The turbulence on the suction surface of the profile is affected by the wall curvature and streamline curvature; near and in the separation region, the streamwise normal Reynolds stress is much larger than that transversal one. None of the turbulence models tested so far can model these important phenomena, but over-predict the Reynolds stresses in the shear layer, and, consequently, predict the separation point too late and the separation zone much too small.

This report treats the implementation of an **A**lgebraic Reynolds **S**tress **M**odel (ASM) into an explicit, compressible, time-marching code. The ASM has the ability to account for curvature effects on the turbulence, as well as for the strong non-isotropy of the turbulence. The code is tested in the flow described above¿

2 The Mean Flow Equations

The mean flow equations that are solved are the continuity equation, the momentum equations and the energy equation. The continuity equation can be written as:

$$\frac{\partial \rho}{\partial t} + \frac{\partial}{\partial x_j}(\rho U_j) = 0$$

The momentum equations and the equation for the total energy have the form:

$$\frac{\partial \rho U_i}{\partial t} + \frac{\partial}{\partial x_j}(\rho U_i U_j) = -\frac{\partial p}{\partial x_i} + \frac{\partial \tau_{ij}}{\partial x_j}$$

$$\frac{\partial \rho e_o}{\partial t} + \frac{\partial}{\partial x_i}[\rho U_i (e_o + p)] = \frac{\partial}{\partial x_i}(\tau_{ij} U_j + \frac{\mu_{eff}}{\sigma_e}\frac{\partial T}{\partial x_i})$$

where the stress tensor is written as:

$$\tau_{ij} = \mu(\frac{\partial U_i}{\partial x_j} + \frac{\partial U_j}{\partial x_i} - \frac{2}{3}\delta_{ij}\frac{\partial U_k}{\partial x_k}) - \rho\overline{u_i u_j}$$

The pressure is obtained from the gas law.

The two-dimensional code used is based on that described in code [14] [18]. The equations are discretized explicit in time. In space using finite volume technique is used using central differencing for the convective terms, stabilized by adding an fourth-order non-homogenous numerical dissipation term [20]. The equations are solved using a four stage Runge-Kutta solver, and local time steps are used to increase the convergence rate.

3 The Algebraic Reynolds Stress Model

3.1 Equations

The exact form of Reynolds stress equation can be written [10]: (the instantaneous Cartesian velocity $\tilde{U}_i$ is divided into a mean part U_i and a fluctuating part u_i so that $\tilde{U}_i = U_i + u_i$; x_i are Cartesian coordinates):

$$\underbrace{U_k \frac{\partial \overline{u_i u_j}}{\partial x_k}}_{C_{ij}} = \underbrace{-\overline{u_i u_k}\frac{\partial U_j}{\partial x_k} - \overline{u_j u_k}\frac{\partial U_i}{\partial x_k}}_{P_{ij}} + \underbrace{\overline{\frac{p}{\rho}(\frac{\partial u_i}{\partial u_j} + \frac{\partial u_j}{\partial u_i})}}_{\Phi_{ij}}$$

$$\underbrace{-\frac{\partial}{\partial x_k}[\overline{u_i u_j u_k} + \overline{\frac{pu_j}{\rho}}\delta_{ik} + + \overline{\frac{pu_i}{\rho}}\delta_{jk} - \nu\frac{\partial \overline{u_i u_j}}{\partial x_k}]}_{D_{ij}} \underbrace{- 2\nu\overline{\frac{\partial u_i}{\partial u_k}\frac{\partial u_j}{\partial u_k}}}_{\varepsilon_{ij}} \quad (1)$$

which symbolically can be written:

$$C_{ij} - D_{ij} \quad = \quad P_{ij} + \Phi_{ij} - \varepsilon_{ij} \quad (2)$$

The exact form of the turbulent kinetic energy equation reads [10], [19]

$$\underbrace{U_j\frac{\partial k}{\partial x_j}}_{C_k} \quad = \quad \underbrace{-\overline{u_i u_j}\frac{\partial U_i}{\partial x_j}}_{P_k} + \underbrace{\overline{\frac{\partial}{\partial x_j}[u_j(\frac{p}{\rho} + \frac{1}{2}u_i u_i)]}}_{D_k} \underbrace{- \nu\overline{\frac{\partial u_i}{\partial u_j}\frac{\partial u_i}{\partial u_j}}}_{\varepsilon}$$

which symbolically can be written:

$$C_k - D_k \quad = \quad P_k - \varepsilon \quad (3)$$

An ASM is a simplified Reynolds Stress Model, where the transport (convective and diffusive) of the Reynolds stresses $\overline{u_i u_j}$ is related to that of the turbulent kinetic energy k, i.e. (see Eqs. 2 and 3)

$$C_{ij} - D_{ij} = \frac{\overline{u_i u_j}}{k}(C_k - D_k) \quad (4)$$

so that Eqs. 2, 3 and 4 give:

$$P_{ij} + \Phi_{ij} - \varepsilon_{ij} = \frac{\overline{u_i u_j}}{k}(P_k - \varepsilon) \quad (5)$$

which, finally, gives

$$\overline{u_i u_j} = \frac{2}{3}\delta_{ij}k + \frac{k}{\varepsilon}\frac{(1-c_2)(P_{ij} - \frac{2}{3}\delta_{ij}P_k) + \Phi'_{ij,1} + \Phi'_{ij,2}}{c_1 + P_k/\varepsilon - 1} \quad (6)$$

where the terms have the following physical meaning:

P_{ij}, P_k are production terms of $\overline{u_i u_j}$ and k, respectively, due to interaction between the mean flow field and the large turbulent structure

Φ_{ij} is the pressure-strain correlation term, which promotes isotropy of the turbulence, by redistributing the normal stresses (decreasing the largest and increasing the smallest), and decreasing the shear stress

ε, ε_{ij} are dissipation (i.e. transformation of mechanical energy into heat in the small-scale turbulence) of k and $\overline{u_i u_j}$, respectively.

3.2 Modelling Assumptions

The production term does not need to be modelled since the mean velocity gradients as well as the Reynolds stresses are calculated. At high Reynolds numbers (i.e. fully turbulent) the small-scale the turbulence is isotropic, which means that the dissipation term ε_{ij} can be assumed to be isotropic, i.e.

$$\varepsilon_{ij} = \frac{2}{3}\varepsilon\delta_{ij}$$

The modelled pressure-strain correlation term Φ_{ij} can be written [19]

$$\Phi_{ij} = \Phi_{ij,1} + \Phi_{ij,2} + \Phi'_{ij,1} + \Phi'_{ij,2}$$

where

$\Phi_{ij,1} = -c_1\frac{\varepsilon}{k}(\overline{u_iu_j} - \frac{2}{3}\delta_{ij}k)$ is due to turbulence fluctuations

$\Phi_{ij,2} = -c_2(P_{ij} - \frac{2}{3}\delta_{ij}P_k)$ is due to both turbulence fluctuations and mean-flow gradients

$\Phi'_{ij,1} = c'_1\frac{\varepsilon}{k}(\overline{u_ku_m}n_kn_m\delta_{ij} - \frac{3}{2}\overline{u_iu_k}n_kn_j - \frac{3}{2}\overline{u_ju_k}n_kn_if(\frac{\ell_t}{x_n})$ is a wall correction term (index n denotes the normal direction). The f-function is a damping function which reduce the effect of the wall correction with increasing distance x_n, and which has the form $f_n = k^{3/2}/(2.55x_n\varepsilon)$.

$\Phi'_{ij,2} = c'_2(\Phi_{km,2}n_kn_m\delta_{ij} - \frac{3}{2}\Phi_{ik,2}n_kn_j - \frac{3}{2}\Phi_{jk,2}n_kn_i)f(\frac{\ell_t}{x_n})$ is the corresponding wall correction term for $\Phi_{ij,2}$.

The resulting wall correction terms for each individual stress are given below.

Wall correction term for $\overline{u^2}$ equation

$$\begin{aligned}\Phi'_{11,1} &= c'_1\frac{\varepsilon}{k}(\overline{v^2}n_y^2 - 2\overline{u^2}n_x^2 - \overline{uv}n_xn_y)f\\ \Phi'_{11,2} &= c'_2(\Phi_{22,2}n_y^2 - 2\Phi_{11,2}n_x^2 - \Phi_{12,2}n_xn_y)f\end{aligned}$$

Wall correction term for $\overline{v^2}$ equation

$$\begin{aligned}\Phi'_{22,1} &= c'_1\frac{\varepsilon}{k}(\overline{u^2}n_x^2 - 2\overline{v^2}n_y^2 - \overline{uv}n_xn_y)f\\ \Phi'_{22,2} &= c'_2(\Phi_{11,2}n_x^2 - 2\Phi_{22,2}n_y^2 - \Phi_{12,2}n_xn_y)f\end{aligned}$$

Wall correction term for $\overline{uv}$ equation

$$\begin{aligned}\Phi'_{12,1} &= \Phi'_{21,1} = -\frac{3}{2}c'_1\frac{\varepsilon}{k}(\overline{uv} + n_xn_y(\overline{u^2} + \overline{v^2}))f\\ \Phi'_{12,2} &= \Phi'_{21,2} = -\frac{3}{2}c'_2(\Phi_{12,2} + n_xn_y(\Phi_{11,2} + \Phi_{22,2}))f\end{aligned}$$

The constant are standard ones [19]: $c_1 = 1.8$, $c_1' = 0.5$, $c_2 = 0.6$, $c_2' = 0.3$.

3.3 Implementation of the ASM

The Reynolds stresses are stored at the cell centres. This is contrary to what normally is done in implicit codes which are based on SIMPLE [13] [17], where the shear stresses are staggered and stored on the faces of the control volumes of the velocities in order to enhance stability. In this work the solution procedure was found to be stable without staggering the shear stresses; this is probably because the mean flow variables are solved *explicitly*, which means that all terms are at the right-hand-side of the discretized equations, and thus the solution procedure is not so sensitive as SIMPLE-methods to the explicit adding of the Reynolds stresses.

The calculation of the Reynolds stresses follows closely that described in [11] and [13]. The equation for the Reynolds stresses, Eq. 6 (inserting the expression for $\Phi_{ij,1}'$ and $\Phi_{ij,2}'$), can be written in matrix form as:

$$\begin{pmatrix} -\overline{u^2} \\ -\overline{v^2} \\ -\overline{uv} \end{pmatrix} = \frac{k}{\varepsilon} \begin{pmatrix} \frac{\alpha_{11}}{\alpha_1}\frac{\partial U}{\partial x} + \frac{\alpha_{11}'}{\alpha_1}\frac{\partial V}{\partial x} & \frac{\alpha_{12}}{\alpha_1}\frac{\partial V}{\partial y} + \frac{\alpha_{12}'}{\alpha_1}\frac{\partial U}{\partial y} & \frac{\alpha_{13}}{\alpha_1}\frac{\partial U}{\partial y} & \frac{\alpha_{14}}{\alpha_1}\frac{\partial V}{\partial x} \\ \frac{\alpha_{21}}{\alpha_2}\frac{\partial U}{\partial x} + \frac{\alpha_{21}'}{\alpha_2}\frac{\partial V}{\partial x} & \frac{\alpha_{22}}{\alpha_2}\frac{\partial V}{\partial y} + \frac{\alpha_{22}'}{\alpha_2}\frac{\partial U}{\partial y} & \frac{\alpha_{23}}{\alpha_2}\frac{\partial U}{\partial y} & \frac{\alpha_{24}}{\alpha_2}\frac{\partial V}{\partial x} \\ \frac{\alpha_{31}}{\alpha_3}\frac{\partial V}{\partial x} + \frac{\alpha_{31}'}{\alpha_3}\frac{\partial U}{\partial x} & \frac{\alpha_{32}}{\alpha_3}\frac{\partial U}{\partial y} + \frac{\alpha_{32}'}{\alpha_3}\frac{\partial V}{\partial y} & \frac{\alpha_{33}}{\alpha_3}\frac{\partial U}{\partial y} & \frac{\alpha_{34}}{\alpha_3}\frac{\partial V}{\partial x} \end{pmatrix} \begin{pmatrix} \overline{u^2} \\ \overline{v^2} \\ \overline{uv} \\ \overline{uv} \end{pmatrix} + \begin{pmatrix} 0 & \frac{\beta_{12}}{\alpha_1} & \frac{\beta_{13}}{\alpha_1} & \frac{\beta_{14}}{\alpha_1} \\ \frac{\beta_{21}}{\alpha_2} & 0 & \frac{\beta_{23}}{\alpha_2} & \frac{\beta_{24}}{\alpha_2} \\ \frac{\beta_{31}}{\alpha_3} & \frac{\beta_{32}}{\alpha_3} & 0 & 0 \end{pmatrix} \begin{pmatrix} \overline{u^2} \\ \overline{v^2} \\ \overline{uv} \\ k \end{pmatrix} \tag{7}$$

Coefficients for $\overline{u^2}$ equation

$$\begin{aligned} \alpha_{11} &= \frac{4}{3}(1-c_2) + c_2c_2'(\frac{8}{3}n_x^2 + \frac{2}{3}n_y^2)f,\ \alpha_{11}' = c_2c_2'n_xn_yf \\ \alpha_{12} &= -\frac{2}{3}(1-c_2) - \frac{4}{3}c_2c_2'f,\ \alpha_{12}' = \alpha_{11}',\ \alpha_{13} = \alpha_{11},\ \alpha_{14} = \alpha_{12} \\ \alpha_1 &= c_1 + \frac{P_k}{\varepsilon} - 1 + 2c_1'n_x^2f \end{aligned}$$

Coefficients for $\overline{v^2}$ equation

$$\alpha_{21} = \alpha_{12},\ \alpha_{21}' = \alpha_{11}',\ \alpha_{22} = \frac{4}{3}(1-c_2) + c_2c_2'(\frac{2}{3}n_x^2 + \frac{8}{3}n_y^2)f$$

$$\alpha'_{22} = \alpha'_{11},\ \alpha_{23} = \alpha_{12},\ \alpha_{24} = \alpha_{22},\ \alpha_2 = c_1 + \frac{P_k}{\varepsilon} - 1 + 2c'_1 n_y^2 f$$

Coefficients for $\overline{uv}$ equation

$$\begin{aligned}
\alpha_{31} &= (1 - c_2) + c_2 c'_2 \frac{3}{2} f,\ \alpha'_{31} = c_2 c'_2 n_x n_y f,\ \alpha_{32} = \alpha_{31} \\
\alpha'_{32} &= \alpha'_{31},\ \alpha_{33} = \alpha'_{31},\ \alpha_{34} = \alpha'_{31},\ \alpha_3 = c_1 + \frac{P_k}{\varepsilon} - 1 + \frac{3}{2} c'_1 f
\end{aligned}$$

Coefficients for the second matrix

$$\begin{aligned}
\beta_{12} &= -c'_1 n_y^2 f,\ \beta_{13} = c'_1 n_x n_y f,\ \beta_{14} = -\frac{2}{3}(c_1 + \frac{P_k}{\varepsilon} - 1) \\
\beta_{21} &= -c'_1 n_x^2 f, \beta_{23} = \beta_{13}, \beta_{24} = \beta_{14} \\
\beta_{31} &= \frac{3}{2} c'_1 n_x n_y f,\ \beta_{32} = \beta_{31}
\end{aligned}$$

3.4 Solution of the Algebraic Reynolds Stress Equations

The main problem when solving equation system in Eq.7 is to ensure the requirement that the normal Reynolds stresses stay positiv during the iteration procedure towards the steady state solution. According to Leschziner [13] this is best achieved by first solving Eq. 7 for the normal stresses and allocate the shear stresses to the right-hand-side, i.e.

$$\begin{pmatrix} a'_{11} & a'_{12} \\ a'_{21} & a'_{22} \end{pmatrix} \begin{pmatrix} \overline{u^2} \\ \overline{v^2} \end{pmatrix} = \begin{pmatrix} c_1 - d_1 \overline{uv} \\ c_2 - d_2 \overline{uv} \end{pmatrix} \equiv \begin{pmatrix} b'_1 \\ b'_2 \end{pmatrix} \tag{8}$$

An efficient way to ensure that $\overline{u^2}$ and $\overline{v^2}$ do not become negative is to ensure that the diagonal elements are positiv and the off-diagonal ones negative. This can be done by allocating *all* terms that are postive to the diagonal elements. For example, the $\overline{u^2}$-equation in Eq. 8 reads

$$a'_{11}\overline{u^2} + a'_{12}\overline{v^2} = c_1 - d_1\overline{uv}$$

where c_1 is positive. Re-writing this equation as explained above gives

$$\begin{gathered}
(max\{a'_{11}, 0\} + max\{a'_{12}\overline{v^2}/\overline{u^2}, 0\} + max\{d_1\overline{uv}/\overline{u^2}, 0\})\overline{u^2} + min\{a'_{12}, 0\}\overline{v^2} = \\
c_1 - min\{d_1\overline{uv}, 0\} - min\{a'_{11}, 0\}\overline{u^2}
\end{gathered}$$

where this is done separately for all terms in a'_{11}, a'_{12}, d_1.

Equation 8 can now be written as

$$\begin{pmatrix} a_{11} & a_{12} \\ a_{21} & a_{22} \end{pmatrix} \begin{pmatrix} \overline{u^2} \\ \overline{v^2} \end{pmatrix} = \begin{pmatrix} b_1 \\ b_2 \end{pmatrix} \tag{9}$$

The a and b coefficients are given below (see Eq. 7).

Coefficients for $\overline{u^2}$ equation

$$
\begin{aligned}
a_{11} &= 1 + \frac{k}{\alpha_1 \varepsilon}[max\{\alpha_{11}\frac{\partial U}{\partial x}, 0\} + max\{\alpha'_{11}\frac{\partial V}{\partial x}, 0\} \\
&\quad + max\{\alpha'_{12}\frac{\partial U}{\partial y}, 0\}\overline{v^2}/\overline{u^2} + max\{\alpha_{12}\frac{\partial V}{\partial y}, 0\}\overline{v^2}/\overline{u^2} \\
&\quad + max\{\alpha_{13}\frac{\partial U}{\partial y}\overline{uv}, 0\}/\overline{u^2} max\{\alpha_{14}\frac{\partial V}{\partial x}\overline{uv}, 0\}/\overline{u^2}] \\
&\quad + \frac{1}{\alpha_1} max\{\beta_{13}\overline{uv}, 0\}/\overline{u^2} \\
a_{12} &= \frac{\beta_{12}}{\alpha_1} + \frac{k}{\alpha_1 \varepsilon}[min\{\alpha_{12}\frac{\partial V}{\partial y}, 0\} + min\{\alpha'_{12}\frac{\partial U}{\partial y}, 0\}]
\end{aligned}
$$

$$
\begin{aligned}
b_1 &= -\frac{\beta_{13}}{\alpha_1}k - \frac{k}{\alpha_1 \varepsilon}[(min\{\alpha_{11}\frac{\partial U}{\partial x}, 0\} + min\{\alpha'_{11}\frac{\partial V}{\partial x}, 0\})\overline{u^2} \\
&\quad + min\{\alpha_{13}\frac{\partial U}{\partial y}\overline{uv}, 0\} + min\{\alpha_{14}\frac{\partial V}{\partial x}\overline{uv}, 0\}] \\
&\quad + \frac{1}{\alpha_1} min\{\beta_{13}\overline{uv}, 0\}
\end{aligned}
$$

Coefficients for $\overline{v^2}$ equation

$$
\begin{aligned}
a_{22} &= 1 + \frac{k}{\alpha_2 \varepsilon}[max\{\alpha_{22}\frac{\partial V}{\partial y}, 0\} + max\{\alpha'_{22}\frac{\partial U}{\partial y}, 0\} \\
&\quad + max\{\alpha_{21}\frac{\partial U}{\partial x}, 0\}\overline{u^2}/\overline{v^2} + max\{\alpha'_{21}\frac{\partial V}{\partial x}, 0\}\overline{u^2}/\overline{v^2} \\
&\quad + max\{\alpha_{23}\frac{\partial U}{\partial y}\overline{uv}, 0\}/\overline{v^2} + max\{\alpha_{24}\frac{\partial V}{\partial x}\overline{uv}, 0\}/\overline{v^2}] \\
&\quad + \frac{1}{\alpha_2} max\{\beta_{23}\overline{uv}, 0\}/\overline{v^2} \\
a_{21} &= \frac{\beta_{21}}{\alpha_2} + \frac{k}{\alpha_2 \varepsilon}[min\{\alpha_{21}\frac{\partial U}{\partial x}, 0\} + min\{\alpha'_{21}\frac{\partial V}{\partial x}, 0\}]
\end{aligned}
$$

$$
\begin{aligned}
b_2 &= -\frac{\beta_{23}}{\alpha_2}k - \frac{k}{\alpha_2 \varepsilon}[(min\{\alpha_{22}\frac{\partial V}{\partial y}, 0\} + min\{\alpha'_{22}\frac{\partial U}{\partial y}, 0\})\overline{v^2} \\
&\quad + min\{\alpha_{23}\frac{\partial U}{\partial y}\overline{uv}, 0\} + min\{\alpha_{24}\frac{\partial V}{\partial x}\overline{uv}, 0\}] \\
&\quad + \frac{1}{\alpha_2} min\{\beta_{23}\overline{uv}, 0\}
\end{aligned}
$$

In order to further stabilize the solution procedure implicit under-relaxation γ is used [11] so that Eq. 9 can be written as

$$\begin{pmatrix} \frac{a_{11}}{\gamma} & a_{12} \\ a_{11} & \frac{a_{22}}{\gamma} \end{pmatrix} \begin{pmatrix} \overline{u^2} \\ \overline{v^2} \end{pmatrix} = \begin{pmatrix} b_1 + \frac{1-\gamma}{\gamma} a_{11} \overline{u^2}_{old} \\ b_2 + \frac{1-\gamma}{\gamma} a_{22} \overline{v^2}_{old} \end{pmatrix} \tag{10}$$

where $\gamma = 0.3$ has been used.

After that the normal stresses have been solved, the shear stress is $\overline{uv}$ is calculated as (see Eq. 7)

$$\overline{uv} = -\frac{k}{\alpha_3 \varepsilon}(\alpha_{31} \frac{\partial V}{\partial x} \overline{u^2} + \alpha_{32} \frac{\partial U}{\partial y} \overline{v^2})$$

which also is under-relaxated as

$$\overline{uv} = (1-\gamma)\overline{uv}_{new} + \gamma \overline{uv}_{old}$$

3.5 The k and ε Equations

Since k and ε appear in the equation for the Reynolds stresses $\overline{u_i u_j}$ in Eq. 6, the equations for k and ε have also to be solved. The standard modellized k and ε-equations in the ASM have the form:

$$\frac{\partial}{\partial x_j}(\rho U_j k) = \frac{\partial}{\partial x_j}[(\mu + c_k \rho \overline{u_j u_m} \frac{k}{\varepsilon}) \frac{\partial k}{\partial x_m}] + P_k - \rho\varepsilon \tag{11}$$

$$\tag{12}$$

$$\frac{\partial}{\partial x_j}(\rho U_j \varepsilon) = \frac{\partial}{\partial x_j}[(\mu + c_\varepsilon \rho \overline{u_j u_m} \frac{k}{\varepsilon} \frac{\partial \varepsilon}{\partial x_m}] + \frac{\varepsilon}{k}(c_{1\varepsilon} P_k - c_{2\varepsilon} \rho\varepsilon) \tag{13}$$

$$P_k = -\rho \overline{u_i u_j} \frac{\partial U_i}{\partial x_j}, \quad c_k = 0.22,\ c_\varepsilon = 0.17,\ c_{1\varepsilon} = 1.44,\ c_{2\varepsilon} = 1.92 \tag{14}$$

Normally the diffusion terms in the k and ε-equations have little influence on the flow field. Calculations modelling these diffusion terms using the eddy viscosity assumption were also carried out, but no noticeable changes in the calulated results were observed.

3.6 Solver for k and ε-equations

Initially, attempts were carried out to solve the k and ε equations explicitly using the existing Runge-Kutta solver. However, no stable, convergent solution was obtained. The main cause for these problems was probably the large source terms. These terms contain the ratio ε/k which in regions of weak turbulence (laminar regions) causes problems since both k and ε tend to zero. Instead we

chosed a implicit discretization method, which has been used for the last 30 years in incompressible codes based on pressure-correction procedures such as SIMPLE [3] [16]. The solution procedure is briefly described below.

The k and ε equations are integrated over a control volume. The diffusive terms are discretized using central differences; hybrid upwind/central differencing is used for the convective terms (details can be found elsewhere [6] [16]). The resulting discretized equations is (Φ denotes k or ε):

$$\begin{aligned}
a_{P,i,j}\Phi_{i,j} &= a_{E,i,j}\Phi_{i+1,j} + a_{W,i,j}\Phi_{i-1,j} + a_{N,i,j}\Phi_{i,j+1} + a_{S,i,j}\Phi_{i,j-1} + S^{\Phi}_{C,i,j} \\
a_{E,i,j} &= max\{-\frac{1}{2}\dot{m}_{i+1/2,j} + D_{I,i+1/2,j}, 0, -\dot{m}_{i+1/2,j}\} \\
a_{W,i,j} &= max\{\frac{1}{2}\dot{m}_{i-1/2,j} + D_{I,i-1/2,j}, 0, \dot{m}_{i-1/2,j}\} \\
a_{N,i,j} &= max\{-\frac{1}{2}\dot{m}_{i,j+1/2} + D_{J,i,j+1/2}, 0, -\dot{m}_{i,j+1/2}\} \\
a_{S,i,j} &= max\{\frac{1}{2}\dot{m}_{i,j-1/2} + D_{J,i,j-1/2}, 0, \dot{m}_{i,j-1/2}\} \\
a_{P,i,j} &= a_{W,i,j} + a_{E,i,j} + a_{S,i,j} + a_{N,i,j} - S^{\Phi}_{P,i,j} \qquad (15)
\end{aligned}$$

where index i,j has been added as to remind that the a- coeffcients and the source terms are matrices.

Index P, E, W, N, S denote Point, East, West, North and South, respectively. $\dot{m}$ denotes mass flux across a cell face, i.e. $\rho\mathbf{U}\cdot\mathbf{S}$ ($\mathbf{S}$=cell face vector area), and $D_{I,i+1/2}(\Phi_{i+1} - \Phi_i$ is the discretized (orthogonal) diffusion along the I-line across the east ($= i+1/2$) cell face, i.e. $(\mu+\mu_t)|\mathbf{S}|\hat{\mathbf{I}}\cdot\nabla$ ($\hat{\mathbf{I}}$ denotes unit vector along the I-line). The source terms contain the generation and dissipation terms (see Eq. 11) as well as the non-orthogonal diffusion.

A tri-diagonal solver is used, and since it solves linear equations along *lines* (say I-line), Eq. 15 is rewritten so that the contributions to point (i,j) from $(i,j-1)$ and $(i,j+1)$ are transferred to the rigth-hand-side, which in matrix form gives

$$\begin{pmatrix}
a_{P,1} & -a_{E,1} & & & & & \\
-a_{W,2} & a_{P,2} & -a_{E,2} & & & & \\
 & & \cdots\cdots\cdots & & & & \\
 & & & -a_{W,i} & a_{P,i} & -a_{E,i} & \\
 & & & \cdots\cdots\cdots & & & \\
 & & & & -a_{W,ni} & a_{P,ni} &
\end{pmatrix}
\begin{pmatrix} \Phi_1 \\ \Phi_2 \\ \cdots \\ \Phi_i \\ \cdots \\ \Phi_{ni} \end{pmatrix}
=
\begin{pmatrix} b_1 \\ b_2 \\ \cdots \\ b_i \\ \cdots \\ b_{ni} \end{pmatrix}$$

where

$$b_i = S_{C,i,j} + a_{N,i,j}\Phi_{i,j+1} + a_{S,i,j}\Phi_{i,j-1}$$

Eliminating all $a_{W,i}$-elements (the lower diagonal) gives

$$\begin{pmatrix} a_{P,1} & -a_{E,1} & & & & \\ & A_{P,2} & -a_{E,2} & & & \\ & & \cdots\cdots\cdots & & & \\ & & & & A_{P,i} & -a_{E,i} \\ & & & \cdots\cdots\cdots & & \\ & & & & & A_{P,ni} \end{pmatrix} \begin{pmatrix} \Phi_1 \\ \Phi_2 \\ \cdots \\ \Phi_i \\ \cdots \\ \Phi_{ni} \end{pmatrix} = \begin{pmatrix} b_1 \\ B_2 \\ \cdots \\ B_i \\ \cdots \\ B_{ni} \end{pmatrix} \quad (16)$$

where

$$B_i = b_i + \frac{a_{W,i} B_{i-1}}{A_{P,i-1}}$$
$$A_{P,i} = a_{P,i} - \frac{a_{W,i} a_{E,i-1}}{A_{P,i-1}} \quad (17)$$

Equation 16 can be written as

$$A_{P,i}\Phi_i - a_{E,i}\Phi_{i+1} = B_i \quad (18)$$

where $A_{P,i}$ and B_i are defined in Eq. 17. The linear equation system in Eq. 15 can now be solved along each I-line by first calculating all $A_{P,i}$ and B_i defined in Eq. 17, and then calculating Φ_{i+1} from Eq. 18.

Above expressions have been derived to solve the linear equation system in Eq. 15 along I-lines. For solving Eq. 15 along J-lines , Eq. 15 is rewritten so that the contributions to point (i, j) from $(i-1, j)$ and $(i+1, j)$ are transferred to the rigth-hand-side, and the subsequent expressions are derived in exactly the same way as above. In this way Eq. 15 can be solved, alternating, along I-lines and J-lines.

At each time step the mean flow equations are solved using the explicit four state Runge-Kutta solver. After that the k-equation is solved twice (once along I- lines and once along J-lines), and the ε-equation is solved twice, and, finally, the Reynolds stresses using ASM are calculated.

3.7 Near-Wall Treatment

Near the walls the one-equation model by Wolfshtein [22], modified by Chen and Patel [5], is used. In this model the standard k equation is solved; the diffusion term in the k-equation is modelled using the eddy viscosity assumption. The turbulent length scales are prescribed as:

$$\ell_\mu = c_\ell n[1 - exp(-R_n/A_\mu)], \;\; \ell_\varepsilon = c_\ell n[1 - exp(-R_n/A_\varepsilon)]$$

(n is the normal distance from the wall) so that the dissipation term in the k-equation and the turbulent viscosity are obtained as:

$$\varepsilon = \frac{k^{3/2}}{\ell_\varepsilon}, \;\; \mu_t = c_\mu \sqrt{k} \ell_\mu \quad (19)$$

The Reynolds number R_n and the constants are defined as

$$R_n = \frac{\sqrt{k}n}{\nu},\ c_\mu = 0.09,\ \ c_\ell = \kappa c_\mu^{-3/4},\ \ A_\mu = 70,\ \ A_\varepsilon = 2c_\ell$$

The one-equation model is used near the walls (for $R_n \leq 250$; the matching line is chosen along a pre-selected grid line), and the standard k and ε-equations in the remaining part of the flow. Since the ASM is not valid near the wall, the Reynolds stresses are here computed using the Boussinesq assumption, i.e.

$$\rho\overline{u_i u_j} = -\mu_t\left(\frac{\partial U_i}{\partial x_j} + \frac{\partial U_j}{\partial x_i} - \frac{2}{3}\delta_{ij}\frac{\partial U_m}{\partial x_m}\right) + \frac{2}{3}\delta_{ij}\rho k \tag{20}$$

where μ_t is calculated using Eq. 19. The matching of the one-equation model and the k and ε- equations does not pose any problems but gives a smooth distribution of μ_t and ε across the matching line. However, the matching of the ASM and the one-equation model gives rise to non- continuity in the Reynolds stresses across the matching line. The one-equation model gives more or less isotropic normal Reynolds stresses according to Eq. 20, whereas ASM gives highly non-isotropic Reynolds stresses, which results in a jump in the profiles of $\overline{u^2}$ and $\overline{v^2}$ across the matching line. Also the $\overline{uv}$-profile is non-smooth across the matching line due to an inconsistency between the one-equation model (or the $k-\varepsilon$ model) and the ASM. In order to illustrate this, a boundary layer flow is chosen where

$$f = 1,\ P_k \simeq \varepsilon,\ P_k = -\overline{uv}\frac{\partial U}{\partial y}$$

so that Eq. 6 gives

$$\overline{v^2} = \frac{2}{3}k\frac{c_1 - 1 + c_2(1-2c_2')}{c_1 + 2c_1'},\ \ -\overline{uv} = \frac{1 - c_2 + \frac{3}{2}c_2c_2'}{c_1 + \frac{3}{2}c_1'}\ \overline{v^2}\ \frac{k}{\varepsilon}\frac{\partial U}{\partial y} \tag{21}$$

Inserting values for the constants gives $-\overline{uv} = 0.065\, k^2/\varepsilon\, \partial U/\partial y$. The coefficient 0.065 should be compared with $c_\mu = 0.09$ which the $k-\varepsilon$ model as well as the one-equation model gives.

The matching problems discussed above do not seem to create any serious problems: the equations remain stable, despite small jumps in the Reynolds stress profiles.

3.8 Transition

Transition was initially imposed by setting $k, \varepsilon, \overline{u^2}, \overline{v^2}, \overline{uv}$ close to zero before the transition point. This resulted in separation on the suction side of the profile where the transition was imposed, probably because this resulted in too an abrupt increase in the viscosity. The transition is presently imposed in a more smooth way. If the transition is to be imposed at x_{tr} the turbulent viscosity is

made to vary linearly in the x-direction between its calculated values at $x_{tr}-\Delta x$ and $x_{tr}+\Delta x$; Δx was taken as 0.05. The same procedure is used on the pressure side with $\Delta_x = 0.1$.

4 Near-wall correction terms

The ASM is used in the present work to calculate the flow around a high-lift airfoil. Some problems regarding the near-wall correction term was encountered, which are decribed in this section.

The near-wall correction terms in simplified form has been used, which is based on the assumption that the walls are parallel to the Cartesian velocity components, which has the form

$$\begin{aligned}\Phi'_{ij,1} &= c'_1\frac{\varepsilon}{k}(\overline{u_n^2}\delta_{ij} - \frac{3}{2}\overline{u_n u_i}\delta_{nj} - \frac{3}{2}\overline{u_n u_j}\delta_{ni})f(\frac{\ell_t}{x_n})\\ \Phi'_{ij,2} &= c'_2(\Phi_{nn,2}\delta_{ij} - \frac{3}{2}\Phi_{ni,2}\delta_{nj} - \frac{3}{2}\Phi_{nj,2}\delta_{ni})f(\frac{\ell_t}{x_n})\end{aligned}$$

This assumption seems to be reasonable, see Fig. 1. However, tests were also carried out using the general formulation [12], and it was found that the contribution from $\overline{u^2}$ in the expression for $\Phi'_{12,1}$ gave a large amplifying effect, which almost cancelled the damping effect due to the $\overline{uv}$-term. The wall correction term $\Phi'_{12,1}$ has the form

$$\Phi'_{12,1} = -c'_1\frac{\varepsilon}{k}\frac{3}{2}[\overline{uv} + (\overline{u^2} + \overline{v^2})n_x n_y]f(\frac{\ell_t}{x_n})$$

and it becomes almost zero on the suction side near the trailing edge (in the separation region). This is due to that the product $n_x n_y$ is not negligible (it reaches values close to 0.2), and that the normal stress $\overline{u^2}$ is much larger than the shear stress. For these reasons the simplified formulation, which does damp the shear stress in the separation region, was used.

5 Computed Results

A C-mesh with 353×65, generated by Chanez and Palicot [4], has been used (see Fig. 1). The near-wall nodes are located at $y^+ \simeq 1$, and 7 to 10 nodes – in the normal direction – are situated in the region $0 \leq y^+ \leq 20$.

The calculated results (for more details, see [7]) are compared with experimental data taken from [2] [9]. The Reynolds number and the Mach number are 2.1×10^6 and 0.15, respectively. Measurements have been carried out in two windtunnels, F1 and F2. In the F1 windtunnel, global characteristics such

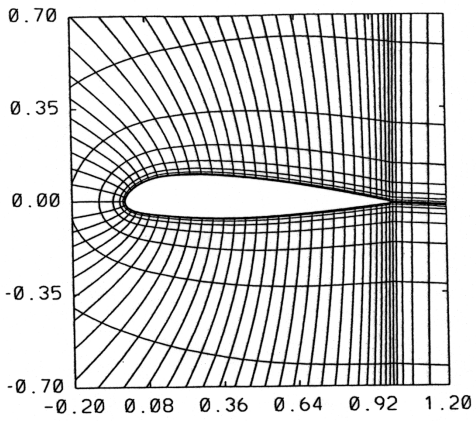

Figure 1: The grid near the profile.

as friction coefficients and surface pressures were measured. The flow field was studied more in detail in the F2 windtunnel, where mean velocity profiles and Reynolds stresses were measured using a three component LDV-system. The blockage effect in the F2 tunnel was more important than in the F1 tunnel, leading to three-dimensional effects for $\alpha \geq 13^o$.

The main motivation for implementing an ASM was that using other lower-order turbulence models such as Baldwin-Lomax or $k-\varepsilon$ models the separation was predicted much too late and the separation zone much too small, and, consequently, no stall was predicted. In Fig. 2 the predicted lift-coefficients using Baldwin-Lomax [4] [15] and the $k-\varepsilon$ model [1] [6] are compared with experimental data [2] [9]. It is seen that the prediced C_L using the Baldwin-Lomax model and the $k-\varepsilon$ model show no tendancies to decrease for increasing angle of attack, whereas the ASM do predict a decrease in C_L at approximately $\alpha = 16^o$ which is in agreement with experiments.

C_L-values in good agreement with experiments. When α is increased, a decrease in C_L is predicted (i.e. approaching stall) for $\alpha = 16.3^o$, which is in agreement with experiments. The point of separation in Table 1 is defined as where the skin-friction changes sign. The ASM seems to predict too large a separation. When the velocity profiles are studied (see below), it will turn out, however, that the separation zone is predicted well in agreement with experiments.

The calculated results are presented below more in detail for $\alpha = 13.3^o$. The main characteristics of the flow is presented in form of c_p and c_F-curves in Fig. 3, and velocity vectors near the trailing edge in Fig. 4. It can be seen that the calculated surface pressure and surface friction agree very well with the experimental values. The U_s-velocities and the shear stresses on the suction side of the airfoil are presented in Fig. 5. Note that in Fig. 5 an orthogonal

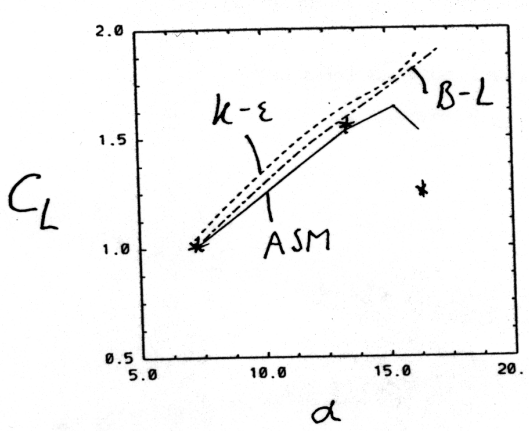

Figure 2: Lift coefficient C_L versus angle of incidence α. ——, ASM; – – – – –, $k-\varepsilon$, — – —, Baldwin-Lomax, $*$, experiments

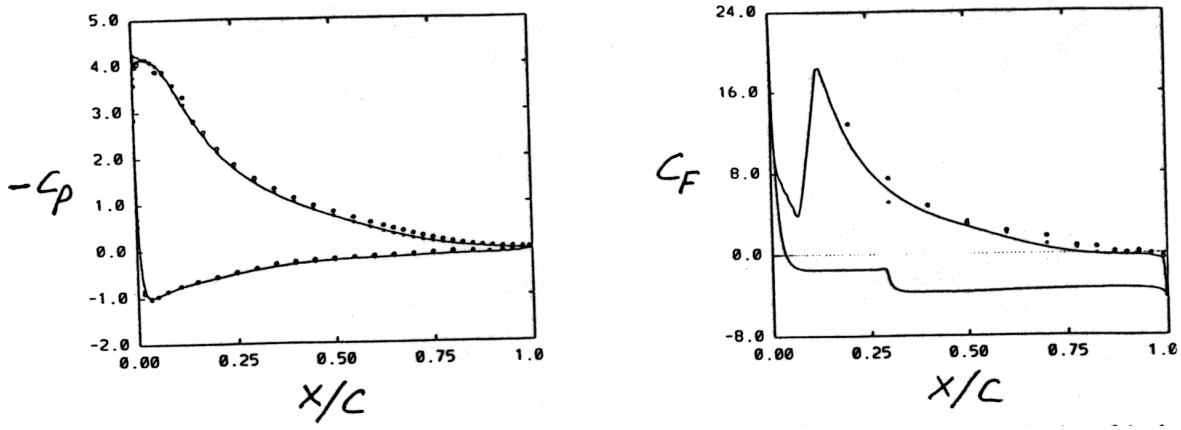

Figure 3: Comparison between calculated and experimental surface pressure and skin friction. $\alpha = 13.3^o$. ——, predictions; markers, experiments (o: F1 windtunnel; $*$: F2 windtunnel).

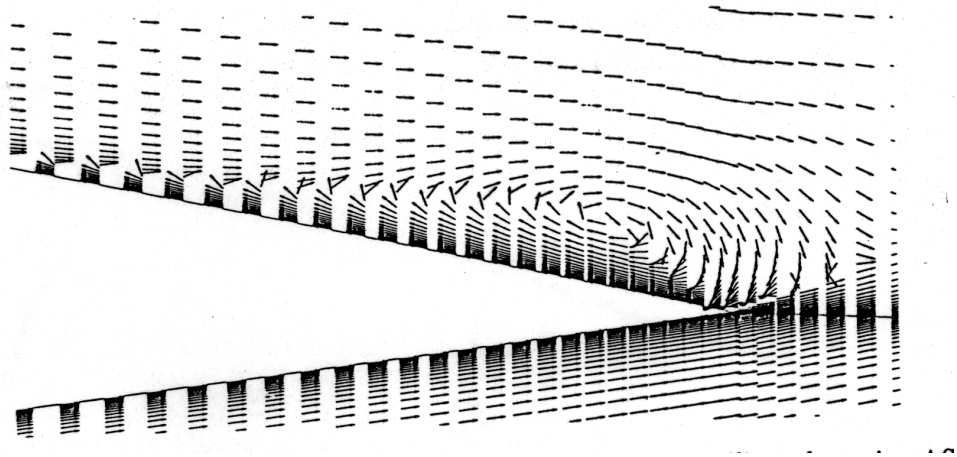

Figure 4: Calculated velocity vectors (constant length) near the trailing edge using ASM.

$s-n$ coordinate system is used. The s-coordinate is tangential to the airfoil, with origin on the surface. The U_s-velocities on the profile are well predicted. The somewhat poorer agreement in the U_s-profiles in the outer part of the shear layer may be due to that the mesh is here rather coarse. As separation is approached, it is seen that the predicted U_s-profiles follow the experimental ones, the profiles getting progressively less full and that an inflextion point in the profiles appears. It can also be seen from Fig. 6 that the anisotropy in the normal Reynolds stresses gets more and more pronounced the trailing edge is approached.

In boundary layer flow the only term which contributes to the production term in the k and ε-equations is $-\overline{u_s u_n}\partial U_s/\partial n$. Thompson and Whitelaw [21] found that near the separation point, as well as in the separation zone, the production term $-(\overline{u_s^2}-\overline{u_n^2})\partial U_s/\partial s$ was of equal importance. In Fig. 7 these terms are presented. At $x/c = 0.2$ the production term due to the normal stresses is not very large (at the most, ten percent of that due to the shear stress). Near the separation point and in the separation region, the two terms are of equal importance. In Fig. 7 the dissipation is also presented, and it is seen that production and dissipation balance each other at $x/c = 0.2$, but that near the separation point and especially in the separation region, this is not the case. The production term using the eddy viscosity assumption $\nu_t(\partial U_s/\partial n)^2$ (the contribution from the normal stresses is negligible) is also included in Fig. 7, which should be compared with $-\overline{u_s u_n}\partial U_s/\partial n$. Note that this is a comparison between the shear stress obtained with the ASM, and that obtained using the eddy viscosity assumption $\overline{u_s u_n} = -\nu_t \partial U_s/\partial n$. It can be seen that the shear stress obtained using the eddy viscosity assumption is considerably larger than that obtained using the ASM. This is because the ASM accounts for the damping

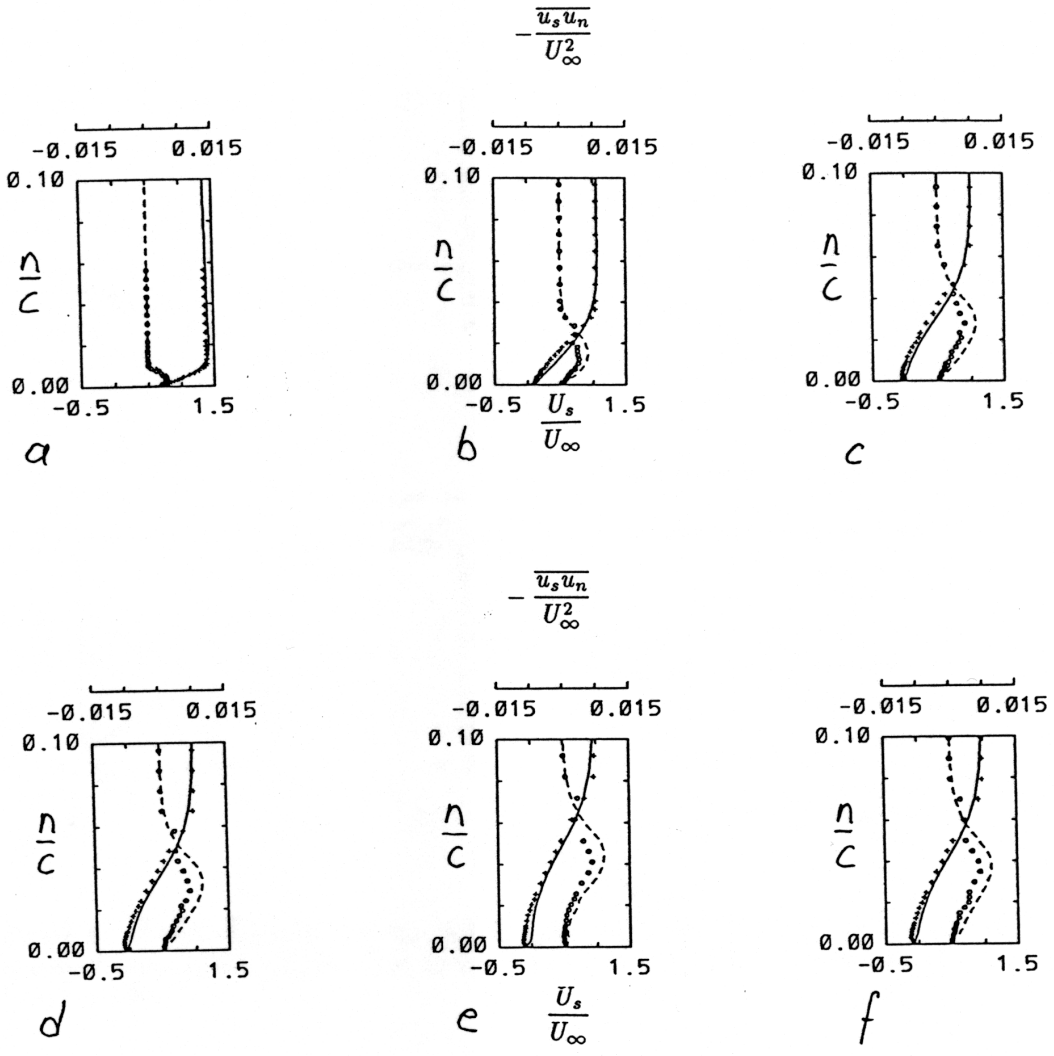

Figure 5: U_s and $-\overline{u_s u_n}$-profiles on the suction side. Solid lines: U_s/U_∞; dashed lines: $-\overline{u_s u_n}/U_\infty^2$; markers: experiments. a) $x/c = 0.4$, b) $x/c = 0.775$, c) $x/c = 0.9$, d) $x/c = 0.93$, e) $x/c = 0.96$, f) $x/c = 0.99$.

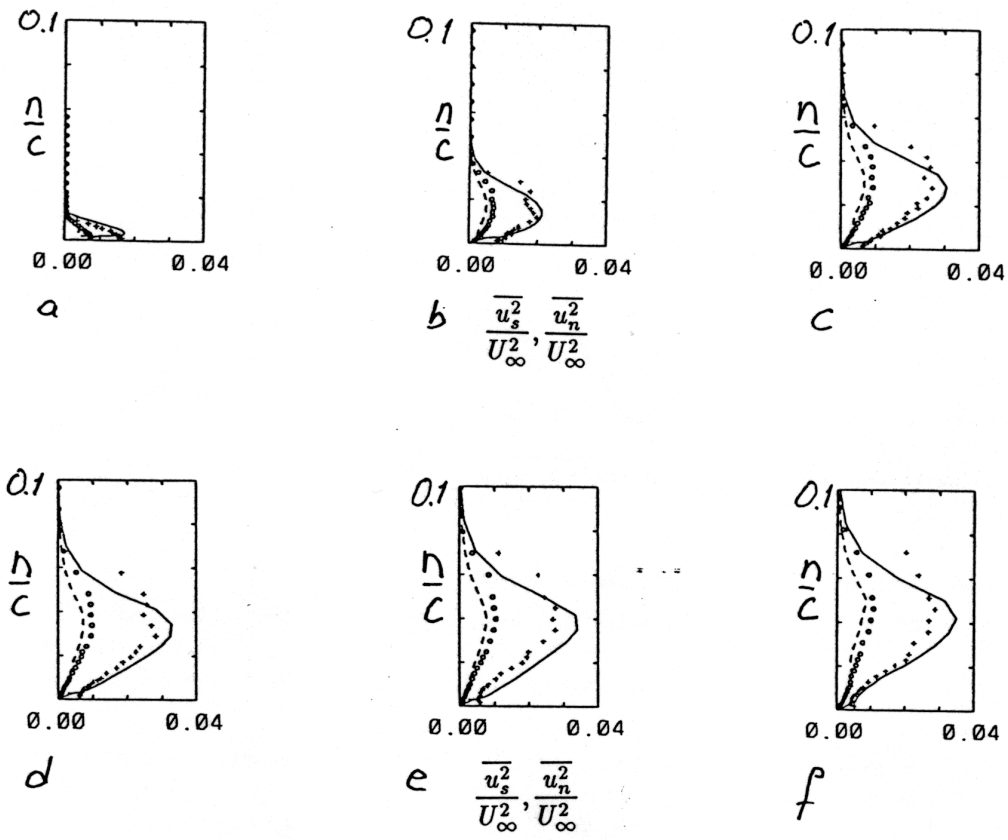

Figure 6: $\overline{u_s^2}$ and $\overline{u_n^2}$-profiles on the suction side. Solid lines: $\overline{u_s^2}/U_\infty^2$; dashed lines: $\overline{u_n^2}/U_\infty^2$; markers: experiments. a) $x/c = 0.4$, b) $x/c = 0.775$, c) $x/c = 0.9$, d) $x/c = 0.93$, e) $x/c = 0.96$, f) $x/c = 0.99$.

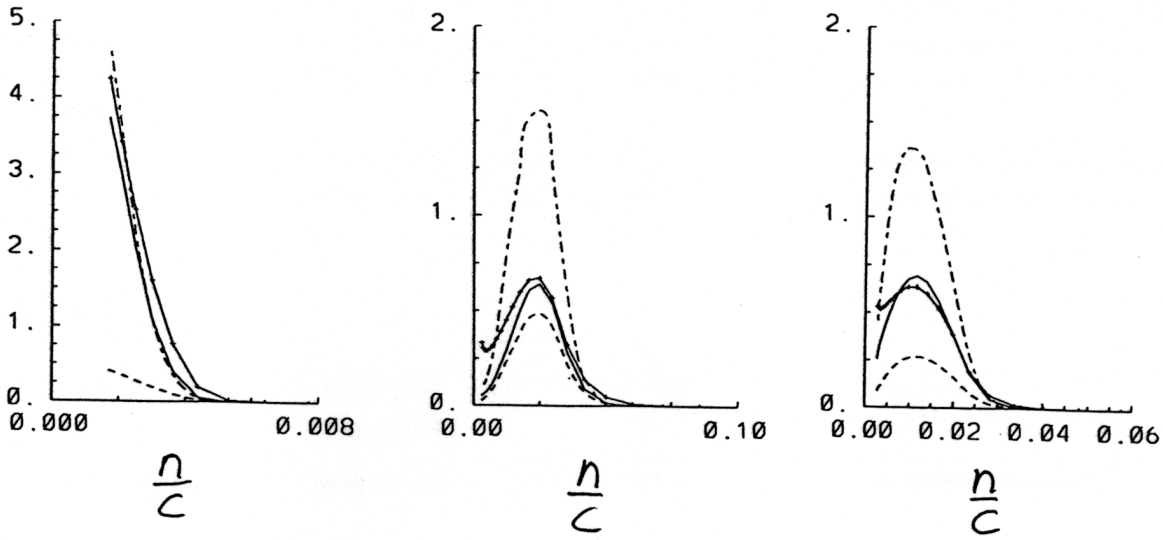

Figure 7: Calculated productions terms in the k- equation.
———, $-\overline{u_s u_n}\partial U_s/\partial n$; − − −−, $(\overline{u_n^2} - \overline{u_s^2})\partial U_s/\partial s$; — - —, $\nu_t[\partial U_s/\partial n]^2$;
—+—+—, ε. a) $x/c = 0.2$, b) $x/c = 0.775$, c) $x/c = 0.9$

of the shear stress and the Reynolds stress normal to the wall; for boundary layer flow the ASM yields, with damping, a c_μ-coefficient of 0.065 (see Eq. 21), which is 28 percent smaller than the c_μ used in $k - \varepsilon$ models.

6 Conclusions

The flow around a two-dimensional high-lift airfoil has been calculated using an algebraic stress turbulence model (ASM), which has been implemented into an existing explicit Runge-Kutta finite volume code. In order to obtain stable and convergent solutions the k and ε-equations – which are calculated when using ASM – are solved with an implicit solver.

As the ASM is only valid for fully turbulent flow it has been matched with a one-equation model close to the wall ($y^+ \leq 50$). This turbulence model has been shown to be able to predict stall for an angle of attack of 16^o, which is in agreement with experiments. Earlier work [1] [6] has shown that $k - \varepsilon$ models are not able to predict stall, and that these models over-predict the shear stress, and consequently predicts separation too late and separation regions too small. The main reasons for the superiority of the ASM are believed to be its ability of taking into account the influence of streamline curvature and the large difference

in the normal Reynolds stresses.

It was found that the general formulation of the near-wall correction terms in the ASM gave too small damping (or none at all) of the shear stress in the separation region. The simplified form – which assumes walls parallel to the Cartesian velocity components – was used, which gave predicted results better in agreement with experiments. It was found, furthermore, that this damping is very important, and that it contributes to the superiority of the ASM over the $k-\varepsilon$ model.

That the near-wall correction term had to be modified in order to give good agreement with experiments, must be considered as a weakness of the ASM. Work is currently going testing a full Reynolds stress model.

Acknowledgements

This work has partly been sponsored by SAAB-SCANIA, Linköping, Sweden.

References

[1] de CAMBRAY, E. - Evaluation d'un modèle $k-\varepsilon$ dans un code Navier-Stokes, Thèse DEA, CERFACS, September, 1990.

[2] CAPBERN, C. and BONNET, C. - Opération décrochage: Rapport Final de Synthèse, Rapport Aerospatiale 443.535./89, Toulouse, 1989.

[3] CARETTA, L.S., GOSMAN, A.D., PATANKAR, S.V., SPALDING, D.B. - Two Calculation Procedures for Steady, Three-Dimensional Flows With Recirculation, Proc. Third Int. Conf. on Numerical Methods in Fluid Dynamics, Vol. 11, p. 60, ed. by Ehlers, Hepp and Weidemüller, 1972.

[4] CHANEZ, Ph. and PALICOT, L. - Évaluation d'un code Navier-Stokes bidimensionnnel pour le calcul de l'écoulement autour d'un profil d'aile, Note interne Aerospatiale, 443.548/90, 1990

[5] CHEN, H.C. and PATEL, V.C. - Practical Near- Wall Turbulence Models for Complex Flows Including Separation, AIAA Paper No 87-1300, Honolulu, June 1987.

[6] DAVIDSON, L. - Implementation of a Semi-Implicit $k-\varepsilon$ Turbulence Model in an Explicit Runge-Kutta Navier-Stokes Code, TR/RF/90/25, CERFACS, 1990.

[7] DAVIDSON, L. - Predicting Stall of a Two-Dimensional Airfoil Using an Algebraic Reynolds Stress Turbulence Model, Rept., CERFACS, 1991.

[8] GENDRE, P. - Computation of Low Speed Flow Around High-Lift Single Element Airfoils With a 2D Navier-Stokes Solver, Proc. Second World

Congress on Computational Mechanics, extended abstracts, pp. 202-205, Stuttgart, 1990.

[9] GLEYZES, C. - Opération décrochage: Résultats de la deuxième campagne d'essais à F2 (mesures de pression et vélocimetrie laser), Rapport Final ONERA/CERT 57/5004.22, Toulouse, 1989.

[10] J.O. HINZE, Turbulence, McGraw-Hill, 2nd ed., 1975.

[11] M. KADJA and M.A. LESCHZINER, THE "TEAM-COG" COMPUTER CODE for Predicting Laminar and Turbulent Flow in Complex Geometries using Curvilinear Orthogonal Grids, Rept., UMIST, Manchester, 1987.

[12] LAUNDER, B.E, REECE, G.J. and RODI, W. - Progress in the Development of a Reynolds-Stress Turbulence Closure, *JFM*, **68**, pp. 537-566, 1975.

[13] LESCHZINER, M.A., Numerical Implementation and Performance of Reynolds-Stress Closures in Finite-Volume Computations of Recirculating and Strongly Swirling Flows, Lecture notes in "Introduction to the Modeling of Turbulence", von Karman Institute for Fluid Dynamics, March 18-21, 1991.

[14] MÜLLER, B. and RIZZI A. - Modelling of Turbulent Transonic Flow Around Aerofoils and Wings, *Comm Appl Num Meth*, **6**, 603-613, 1990.

[15] PALICOT, L. - Sensibilité à divers parametres d'un code Navier-Stokes bidimensionnel appliqué au calcul d'un profil d'aile, Note interne Aerospatiale, 443.581/90, 1990

[16] PATANKAR, S.V. - Numerical Heat Transfer and Fluid Flow, McGraw-Hill, New York, 1980.

[17] POPE, S.B. and WHITELAW, J.H. - The Calculation of Near-Wake Flows, *JFM*, **73**, pp. 9-30, 1976.

[18] RIZZI A. and MÜLLER, B. - Large-Scale Viscous Simulation of Laminar Vortex Flow Over a Delta Wing, *AIAA Journal*, **27**, 833- 840, 1989.

[19] RODI, W. and SCHEUERER, G. - Calculation of Curved Shear Layers With Two-Equation Turbulence Models, *Phys. Fluids*, **26**, No. 6, pp. 1422-1435, 1983.

[20] SWANSON, R.C. and TURKEL, E. - Artificial Dissipation and Central Difference Schemes for the Euler and Navier-Stokes Equations, AIAA Paper No 87-1107, 1987.

[21] THOMPSON, B.E. and WHITELAW, J.H. - Characteristics of a Trailing-Edge Flow With Turbulent Boundary-Layer Separation, *JFM*, **157**, pp. 305-326, 1985.

[22] WOLFSHTEIN, M. - The Velocity and Temperature Distribution in One-Dimensional Flow with Turbulence Augmentation and Pressure Gradient, *Int. J. Mass Heat Transfer*, **12**, pp. 301-318, 1969.